

**Automated and accurate protein structure description:  
Distribution of Ideal Secondary Structural Units in Natural Proteins**

Sushilee Raganathan,<sup>a</sup> Dmitry Izotov,<sup>a</sup> Elfi Kraka,<sup>a</sup> and Dieter Cremer<sup>a,b,\*</sup>

<sup>a</sup>Department of Chemistry, University of the Pacific  
3601 Pacific Ave., Stockton, CA 95211-0110

<sup>b</sup>Department of Physics, University of the Pacific  
3601 Pacific Ave., Stockton, CA 95211-0110

**Abstract:** A new method for the Automated Protein Structure Analysis (APSA) is derived, which simplifies the protein backbone to a smooth curve in 3-dimensional space. For the purpose of obtaining this smooth line each amino acid is represented by its C<sub>α</sub> atom, which serves as suitable anchor point for a cubic spline fit. The backbone line is characterized by arc length  $s$ , curvature  $\kappa(s)$ , and torsion  $\tau(s)$ . The  $\kappa(s)$  and  $\tau(s)$  diagrams of the protein backbone suppress, because of the level of coarse graining applied, details of the bond framework of the backbone, however reveal accurately all secondary structure features of a protein. Advantages of APSA are its quantitative representation and analysis of 3-dimensional structure in form of 2-dimensional curvature and torsion patterns, its easy visualization of complicated conformational features, and its general applicability. Typical differences between  $3_{10}$ -,  $\alpha$ -,  $\pi$ -helices, and  $\beta$ -strands are quantified with the help of the  $\kappa(s)$  and  $\tau(s)$  diagrams. For a test set of 20 proteins, 63 % of all helical residues and 48.5 % of all extended residues are identified to be in ideal conformational environments with the help of APSA. APSA is compared with other methods for protein structure analysis and its applicability to higher levels of protein structure is discussed.

*key words:* protein structure, protein backbone, curvature, torsion, secondary structure, helices,  $\beta$ -sheets

## 1. Introduction

Protein structure is organized into primary, secondary, tertiary, and quaternary levels expressing in this way its enormous variety and complexity. [1] There have been numerous attempts of simplifying measured structures for the purpose of finding unique conformational patterns. For example, Venkatachalam [2] presented a local description of a protein molecule based merely on the polypeptide chain backbone. Furthermore, he showed that just two of the three conformational angles of the backbone have to be specified for a particular amino acid residue because conjugative effects keep the peptide unit planar. [2] These simplifications do not hinder the valid description of a protein, but confirm earlier predictions [1] of its periodical structure in agreement with crystallographic data. [3] A different approach employed by Kabsch and Sander [4] described secondary structures in terms of the shape and organization of hydrogen-bonded rings found along the backbone. They were able to identify helices and beta sheets quickly and precisely. A higher level of organization that involved pairs of secondary structures called the supersecondary structures was identified by Rao and Rossman [5] by comparison of protein structures. These and other methods were applied for protein structure description, always with the objective of developing appropriate tools for protein structure prediction. From an elementary point of view one can distinguish between three different approaches to fulfill these objectives. One can base protein structure analysis and prediction exclusively on conformational (geometrical) features. Alternatively, one can correlate structural features with amino acid properties such as H-bonding ability, hydrophilicity, hydrophobicity, polarity, etc. [1] and use the latter properties for structure classification. Finally, a combination of conformational (geometrical) and physiochemical amino acid properties can be used for the purpose of structure analysis and prediction.

Based on various such descriptions, secondary structure elements like helices and  $\beta$  sheets, supersecondary structures like hairpins and corners, larger supersecondary motifs like the beta barrel and folds of domains in globular proteins have been extensively classified. [1] Classification of proteins deposited in the Protein Data Bank (PDB) [6] can be found in databases such as SCOP [7], CATH [8], DALI [9], etc., which combine automated and manual sorting of domains. Such domain classifications have been compared and analyzed [10] and it has been shown that they are frequently conflicting with regard to domain definition and assignment of domain boundaries. Conflicting descriptions can also be obtained when using secondary structure assignment programs such as DSSP [4], STRIDE [11], DEFINE [12], and KAKSI [13] (for a comparison, see Ref. [13]). It requires detailed and individual analysis of structures at specific localized sites to classify some of the loop regions and show them to be made up of simpler units [14,15]. More recently, secondary structure has been analyzed on the basis of neural networks. [16] In general, modern secondary structure assignment and prediction can refer to a multitude of strategies based on H-bonding [4], backbone conformation [2], multiple sequence alignments [17], energy based evaluations [18], etc.

It is generally accepted that one can recognize protein structure from the form of its backbone. [1,2] Once the backbone structure is understood, one can complete the backbone by adding side chains using available

procedures. [19] Despite such accomplishments, the need for improved analysis of backbone structure is mentioned [20] in connection with protein structure predictions and when elucidating protein functionality. [1] Hence an automated systematic description of the backbone structure of a protein, is still, after many decades of protein studies, a needed tool to relate protein primary structure to protein functionality. The state of the art in protein structure description is often judged in view of its value for protein structure prediction where the efficiency of automation plays a major role. [21]

Any useful description of backbone or total protein structure has to consider the different levels of structural description, which lead from the secondary elements through the supersecondary units and motifs to the tertiary level with folds of domains. [1] This hierarchy of structural descriptors implies that for any given point of a protein backbone an increasingly larger environment has to be taken into account to step up from a purely local to a global description. Clearly, any complete description of the protein backbone must include all levels of the structural hierarchy. One could assume that after 50 years of research in this field at least the secondary level of protein structure is well-understood; however this is questionable given that even helices are still under evaluation. [22,23]

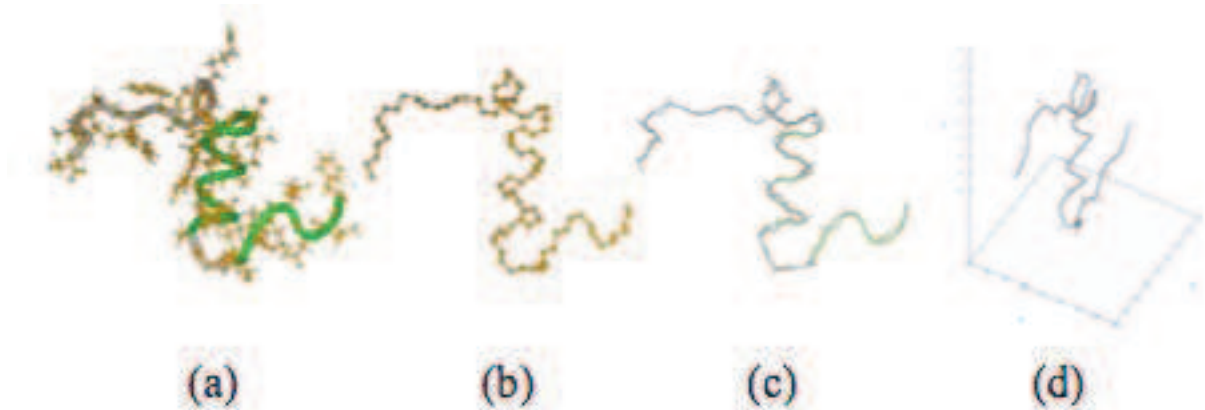


**Figure 1.** Simplification of the protein structure to a smooth line in 3D-space in 3 steps. (a) Perspective drawing of the structure of insulin B chain taken from PDB file 1JCO. [6] (b) After deleting all side chains the backbone of insulin B chain becomes visible. The  $C_{\alpha}$  atoms of all residues are indicated by dots. (c) The positions of the  $C_{\alpha}$  atoms are connected by a cubic spline fit. (d) The backbone is represented as a smooth line in 3D-space.

In this work, we will approach the task of describing protein structure in the spirit of early structural simplifications. We will delete all side chains and focus just on the protein backbone (Figures 1a to 1d). The orientation of the backbone in 3-dimensional (3D) space can be determined by a multitude of residue dihedral angles  $\phi$  and  $\psi$ . However, such an approach leads to a local and discrete description of the backbone that,

only with difficulties, can be applied for the description of tertiary structure. For the purpose of developing a simpler approach to protein structure description we introduce two strategies:

a) We sacrifice a fine-grained atom-by-atom description of the backbone leading to excessive detail to a coarse-grained one. The latter can be done in various steps with the purpose of including increasingly more non-local structural features into the protein description. At the level used in this work, each residue is represented by just one anchor point (Figure 1c). At higher levels of coarse graining, one would have to present supersecondary or tertiary structural units by new anchor points to add more non-local features to the protein description. In this way, all features from secondary to tertiary structure become accessible to a purely conformational (geometric) approach of structure description.

b) The second feature of the current approach is based on a continuous rather than discrete representation of the protein backbone. We convert the latter into a smooth line oriented in 3D space by the anchor points of step (a). Along this line, we use three mathematical parameters to determine length and orientation of the backbone line, namely the arc length  $s$ , the scalar curvature  $\kappa$ , and the scalar torsion  $\tau$ . By expressing  $\kappa$  and  $\tau$  as a function of the arc length  $s$  we obtain a continuous representation of the protein backbone (see Figure 1d), which adopts characteristic patterns for given structural features of a protein. The advantages of such a strategy lie in its ease of automation in form of a computer program, its general applicability, and the mathematical accuracy of structure description, as will be shown in this work.

A detailed and systematic presentation of the approach sketched above and results obtained with it are given in the following sections. In Section 2, mathematical procedures and the data set used in this work are described. Results and discussion will be presented in Section 3. Section 4 is devoted to a comparison of the current method with other methods of protein structure description and prediction. Finally, we will summarize the most important conclusions of this work and provide an outlook on the next steps of this work.

## 2. Computational methods and procedures

As described in the introduction, the protein backbone can be presented as a smooth regularly parameterized space-curve. Any sufficiently smooth curve in 3D space is completely characterized by three parameters including its arc length  $s$ , scalar curvature  $\kappa$ , and scalar torsion  $\tau$  where  $\kappa$  and  $\tau$  are expressed as a function of  $s$ . [24] In Figure 2, tangent vector  $\mathbf{t}$ , normal vector  $\mathbf{n}$  (in applications also called curvature vector), and binormal vector  $\mathbf{b}$  of a Frenet frame at point  $P_1$  of a left-handed helix curve  $\mathbf{r}(s)$  are shown. If the Frenet frame moves along the curve to point  $P_2$ ,  $\mathbf{t}$ ,  $\mathbf{n}$ , and  $\mathbf{b}$  readjust their orientation where the rotation of the Frenet frame around vectors  $\mathbf{b}$  and  $\mathbf{t}$  is given by curvature and torsion. The formulas for the latter quantities expressed as a function of the arc length  $s$  are: [24]

$$\kappa(s) = |\mathbf{r}''(s)|, \tag{1}$$

$$\tau(s) = \frac{\langle \mathbf{r}'(s), \mathbf{r}''(s), \mathbf{r}'''(s) \rangle}{|\mathbf{r}''(s)|^2}, \quad (2)$$

where  $|\cdot|$  is the norm, and  $\langle \cdot \rangle$  is the triple product.

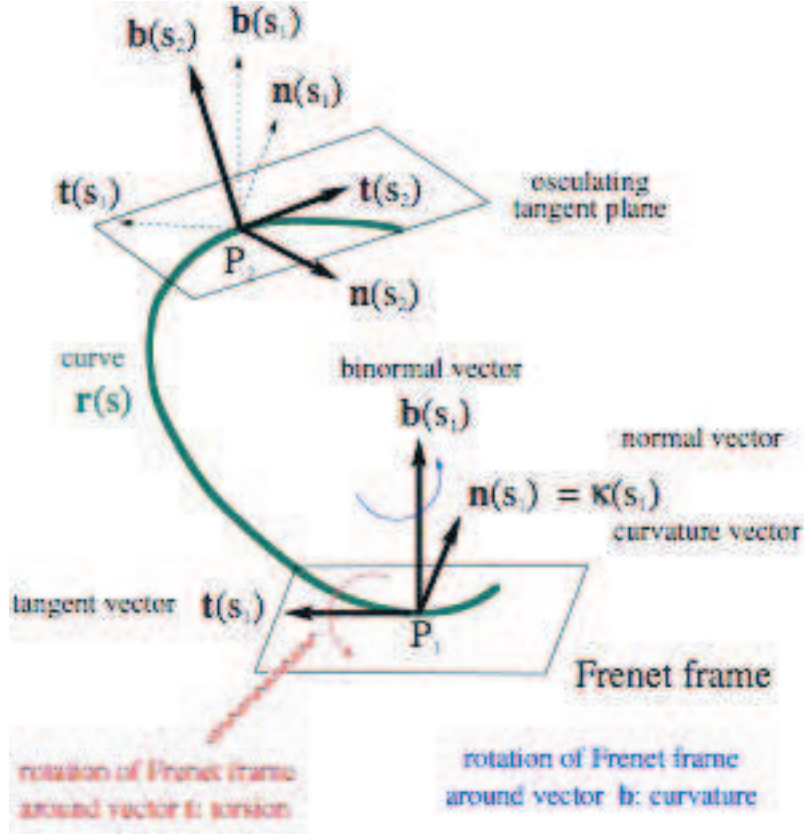


**Figure 2.** Schematic representation of tangent  $\mathbf{t}(s)$ , normal  $\mathbf{n}(s)$ , and binormal vector  $\mathbf{b}(s)$  vector of a Frenet frame at points  $P_1$  and  $P_2$  of curve  $\mathbf{r}(s)$  presenting part of a left-handed helix. The normal vector is often also called curvature vector. Movement of the Frenet frame leads to an osculating tangent plane, a rotation at the tangent vector  $\mathbf{t}(s)$  (indicated by a red arrow), and a rotation at the binormal vector  $\mathbf{b}(s)$  (blue arrow) thus specifying torsion and curvature, respectively. For point  $P_2$ , the old Frenet frame (dashed arrows) and the new Frenet one (bold arrows) are given, which reveals that the torsion is negative according to a left-handed twist of the Frenet frame around  $\mathbf{t}$ .

For the purpose of converting the framework of bonds establishing the backbone into a smooth 3D line one has to answer two questions. a) What are the most suitable anchor points for the representation of the backbone? - b) What type of spline function should be used? - The first question relates to the coarse graining strategy outlined in the introduction. If all backbone atoms would be used as anchor points an excessively detailed description of local conformational features with strongly oscillating scalar curvature and torsion would result thus losing the chance of describing non-local features of protein structure. Instead, we have to apply a first level of coarse graining by presenting each residue along the backbone just by one

anchor point. In this way, a smoother more global presentation of the backbone can be obtained sacrificing unnecessary structural details such as the individual orientation of residue bonds in 3D-space.

There are various choices for the anchor points. These could involve the N or C(=O) atoms of the peptide linkages, alternatively the C $_{\alpha}$  atoms, or any geometric point of a residue (center of mass, geometric center, etc.). After testing four alternatives (N, C(=O), C $_{\alpha}$ , midpoints of C $_{\alpha}$  atom-pairs), we came to the conclusion that protein structure is best presented at the first level of coarse graining by utilizing the C $_{\alpha}$  atoms as anchor points. The conformational flexibility of the protein backbone is primarily determined by the C $_{\alpha}$  atoms and less by the atoms of the peptide linkage. Hence, any description of protein conformation should reflect the position of the C $_{\alpha}$  atoms in 3D space. This is in line with the fact that from the early  $\phi - \psi$ - Ramachandran plots [2] to more recent models of protein folding [25], geometrical descriptions of the protein backbone have repeatedly reverted to C $_{\alpha}$ -based representations. In the same spirit, graphical representations of proteins indicating secondary structure preferentially utilize the C $_{\alpha}$  positions in 3D space. [26]

It has to be noted that the choice of the anchor points relates to some degree to the choice of the polynomial functions selected to represent the protein backbone. Of several possible spline functions that can be used for this purpose, the cubic spline was found most suitable, owing to its simplicity. It is uniquely defined by the requirement of smoothness at the anchor points (C $_{\alpha}$  atoms) and by two boundary conditions (see below). In addition, it corresponds to a curve with minimum deformation energy. Other types of splines do not have this physical property; moreover, the higher-order splines often require extra, nonphysical constraints, as they need more parameters to be fixed. Whereas the cubic spline functions have a well-defined advantage when used with the C $_{\alpha}$  anchor points, their use in connection with the N, the carbonyl C atoms or the mid-points of C $_{\alpha}$  atom-pairs does not lead to smooth backbone patterns in terms of curvature and torsion of secondary structures.

The cubic spline functions used in this work employ *natural* boundary conditions at either end, i.e., the curvature  $\kappa$  is fixed to zero at the terminal C $_{\alpha}$  atoms of a protein. This approximation is reasonable considering the high conformational flexibility of the ends of most proteins, which are not associated with a constant  $\kappa$  value. Test calculations (see Appendix I) revealed that the first and the last two residues of the protein backbone are affected by the boundary conditions and therefore they are excluded from the analysis.

The accuracy of the representation of the protein backbone by a spline function depends in turn on the accuracy of the coordinates supplied. Therefore, the sensitivity of the cubic spline interpolation to any uncertainty in coordinates has been quantified. The analysis reveals that at the first level of coarse graining (with the C $_{\alpha}$  atoms as anchor points) calculated  $\kappa(s)$  and  $\tau(s)$  values are more accurate than  $0.1 \text{ \AA}^{-1}$  as long as the resolution  $R$  of the protein coordinates is  $\leq 2 \text{ \AA}$ .

The new Automated Protein Structure Analysis (APSA) method is carried out utilizing a program that extracts the  $C_\alpha$  coordinates from a PDB file, [6] calculates the protein backbone line, determines  $\kappa(s)$  and  $\tau(s)$ , and then, utilizing a set of predefined rules coined from ideal secondary structure patterns of  $\kappa(s)$  and  $\tau(s)$ , automatically analyzes and identifies all secondary structural features of the protein considered. Curvature values are always positive whereas torsion values can be both positive and negative. The sign of the scalar torsion is defined by the rotation of the binormal vector  $\mathbf{b}$  around the tangent vector of the curve. If it is clock-wise (along a right-handed screw), the torsion is positive; otherwise it is negative as in the case of the left-handed helix of Figure 2. Equation (2) implicitly includes the direction of the rotation of the binormal vector and, hence, the sign of the torsion. Given that APSA analyzes proteins from the first residue at the N-terminus, any change of sign of  $\tau(s)$  correctly reflects any change of chirality of a protein helix or any other structural unit.

In this work, APSA is used to investigate ideal secondary structural units of proteins. Suitable references for the latter were constructed with the help of an 18-residue polyalanine helix and  $\beta$ -strand. For this purpose, ideal  $\phi$  and  $\psi$  angles of  $-57^\circ$  and  $-47^\circ$  for the  $\alpha$ -helix,  $-49^\circ$  and  $-26^\circ$  for the  $3_{10}$  helix, and  $-57^\circ$  and  $-70^\circ$  for the  $\pi$  helix were used. A left handed  $\alpha$ -helix was constructed using the ideal backbone angles  $\phi$  and  $\psi$  of  $60^\circ$  and  $54^\circ$ . An ideal  $\beta$  strand is not planar as it is often sterically influenced by neighboring structures and therefore, it resembles a twisted stretched ribbon. This effect was modeled using  $\phi$  and  $\psi$  angles of  $-120^\circ$  and  $120^\circ$ .

The speed and the reliability of APSA’s assignments were tested on a dataset of 20 proteins from the PDB [6] listed in Table 1. Only X-ray structures having a refinement of about 2 Å or less were selected. Structure breaks and proteins with alternate locations provided for  $C_\alpha$  positions were avoided though the  $\kappa(s)$  and  $\tau(s)$  patterns did not differ much in these cases. The set of proteins used for the APSA description contained different sized proteins with various lengths of helices and  $\beta$  sheets, connected by small and large sized loop regions. The CATH classification system [8] was followed making sure that the protein examples chosen spread over the main classes.

### 3. Analysis of Ideal Secondary Structures

Table 1 contains the set of 20 proteins investigated in this work and summarizes the number of secondary structures and residues in ideal conformational environments contained in these proteins. In Table 2, Figure 3, and Figure 4, suitable references of  $\kappa(s)$  and  $\tau(s)$  values (and diagrams) of ideal secondary structures formed by 18-residue long polyalanines (right-handed ideal  $3_{10}$ ,  $\alpha$ -, and  $\pi$ -helix in Figure 3a and Figure 4, left-handed  $\alpha$ -helix in Figure 3b; *ideal*  $\beta$  strands in Figure 3c) are given.

Table 1: The number of ideal  $\alpha$ -helices,  $\beta$ -strands, and the corresponding number of amino acids (in parentheses) in ideal environments as found among 20 proteins using strict  $\kappa$ - $\tau$  ranges from Table 2. The assignment by DSSP is given for comparison.<sup>a</sup>

#	Protein Name	Resolution (Å)	PDB ID	$\alpha$ -Helices APSA	$\beta$ -Strands APSA	$\alpha$ -Helices DSSP	$\beta$ -Strands DSSP
1.	Crambin	1.50	1CRN	2 (13)	3(4)	2(19)	0
2.	Lysozyme	1.82	1HC0	5(26)	3(5)	7(53)	2(6)
3.	Mmp9 Haemopexin domain,	1.95	1ITV	1(5)	15(37)	2(8)	15(83)
4.	Flavocytochrome C3 (S. frigidimarina)	1.80	1KSS	18(123)	17(40)	20(187)	19(100)
5.	Lambda Repressor	1.80	1LMB	6(45)	1(0)	5(59)	0
6.	Pumilio - Homology Domain	1.90	1M8Z	21(113)	0	28(237)	0(0)
7.	Peridinin-Chlorophyll-Protein (A carterae)	2.00	1PPR	17(186)	2(1)	14(220)	0
8.	Bence Jones Protein	2.00	1REI	0	9(19)	0	9(49)
9.	Elastase (P. aeruginosa)	1.40	1U4G	12(79)	10(19)	8(110)	6(27)
10.	Ubiquitin	1.80	1UBQ	1(11)	5(8)	1(12)	5(24)
11.	Uteroglobin	1.34	1UTG	4(32)	1(0)	4(50)	0
12.	Adenylate Kinase	1.85	2AK3	9(67)	10(21)	8(101)	7(31)
13.	Carbonate Dehydratase	2.00	2CAB	2(8)	18(38)	3(17)	16(79)
14.	Citrate Synthase	1.70	2CTS	22(140)	10(8)	20(257)	2(6)
15.	Flavodoxin semiquinone	1.80	2FOX	4(38)	7(22)	5(50)	5(27)
16.	Hemoglobin (Horse)	2.00	2MHB	11(71)	1(0)	7(95)	0
17.	Prealbumin (Human plasma)	1.80	2PAB	1(3)	9(26)	1(8)	7(55)
18.	Porin	1.80	2POR	1(4)	16(78)	3(17)	16(171)
19.	Aspartate Aminotransferase	1.90	7AAT	13(135)	12(20)	16(185)	9(48)
20.	Papain	1.65	9PAP	4(35)	10(12)	5(49)	6(32)
	<b>TOTAL</b>			<b>155(1134)</b>	<b>159(358)</b>	<b>159(1744)</b>	<b>124(738)</b>

<sup>a</sup> Only 65 % (among  $\alpha$  helical residues) and 48.5% (among  $\beta$ -strand residues) occur in ideal environments.





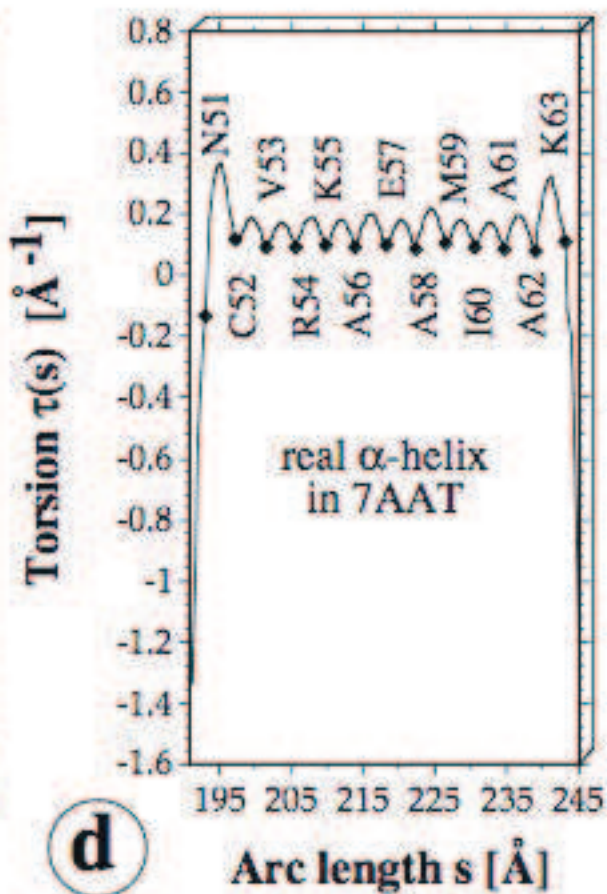
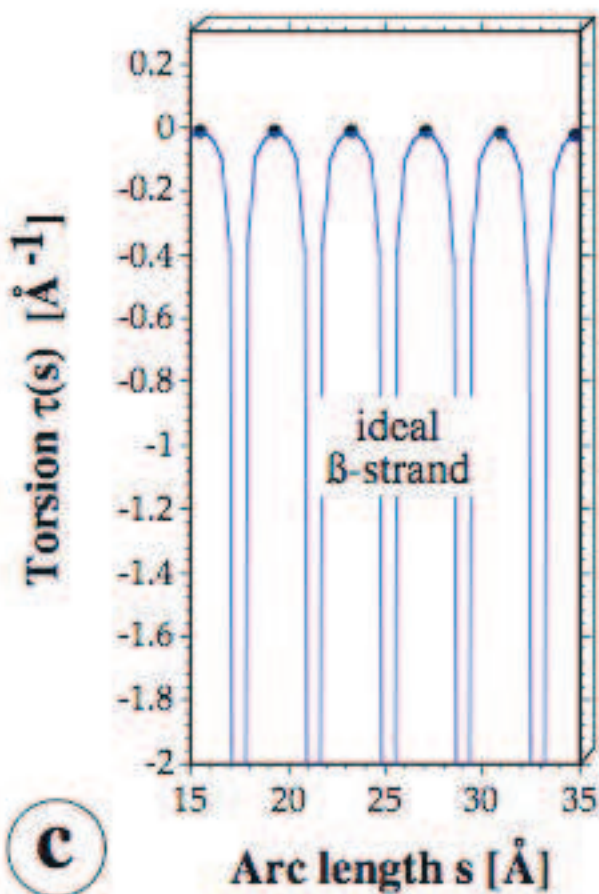
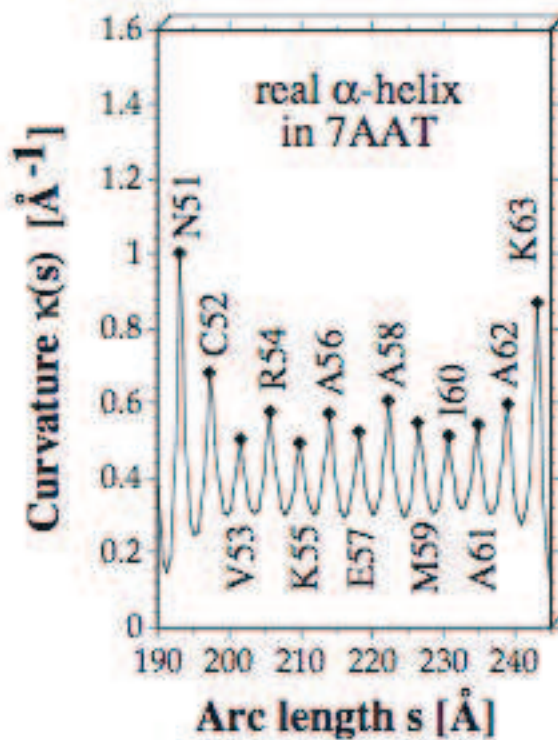
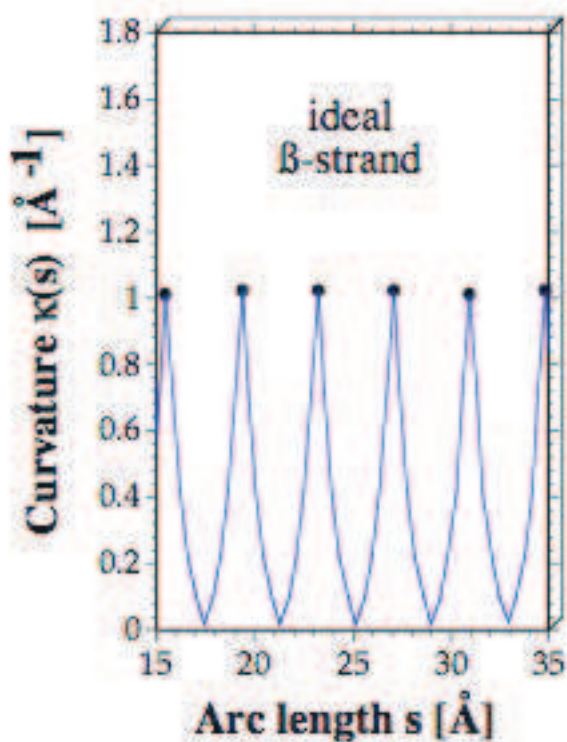


**Figure 3.** Curvature diagrams  $\kappa(s)$  (above) and torsion diagrams  $\tau(s)$  (below) of (a) right-handed ideal  $3_{10}$ ,  $\alpha$ -, and  $\pi$ -helix; (b) left-handed ideal  $\alpha$ -helix, (c) ideal  $\beta$ -strand; (d) natural  $\alpha$ -helix from N51 to K63 in protein 7AAT [6]; (g) natural  $\beta$ -strand from T17 to K23 in protein 2SOD. [6]

An ideal helix has constant curvature and torsion values; for example, for a diameter of  $1.0 \text{ \AA}$ ,  $\kappa(s) = 0.5 \text{ \AA}^{-1}$ . For the ideal 18-residue long polyalanine, the three types of ideal helices have different  $\kappa(s)$  and  $\tau(s)$  patterns, which can be distinguished qualitatively and quantitatively (Figure 3a). The differences in  $\kappa(s)$  and  $\tau(s)$  values correspond to the differences in pitch and diameter of each helix. Since a  $3_{10}$  polyalanine helix has an  $i \rightarrow i+3$  H-bonding pattern (first and third residues are connected by a  $\text{C=O} \cdots \text{H-N}$  bond), the diameter of a  $3_{10}$ -helix is smaller than that of an  $\alpha$ -helix. Only 3 residues form a turn (each residue corresponds to a  $120^\circ$  turn) giving a translation step of  $2.0 \text{ \AA}$  (along the helix axis for one loop). Clearly, the tighter  $3_{10}$ -helix must have larger curvature and torsion oscillations than the  $\alpha$ -helix (Figure 3a). For the  $\alpha$ -helix, the  $i \rightarrow i+4$  H-bonding pattern, results in 3.6 residues per turn where a residue leads to a  $100^\circ$  turn and the translation step is  $1.5 \text{ \AA}$ . The  $\pi$ -helix is characterized by the  $i \rightarrow i+5$  H-bonding pattern, 4.1 residues per turn, a  $87^\circ$  turn per residue, and a translation step of  $1.15 \text{ \AA}$ . Hence, oscillations in curvature and torsion are smallest for the  $\pi$ -helix and intermediate for the  $\alpha$ -helix. Considering the reduction in the diameters and the transversion step of  $3_{10}$ ,  $\alpha$ -, and  $\pi$ -helix in that order, the amplitude of oscillation in the curvature and torsion must decrease as seen from the  $\kappa(s)$  and  $\tau(s)$  diagrams of Figure 3a.

The functions  $\kappa(s)$  and  $\tau(s)$  oscillate about an average value, which is an innate property of the helix in question:  $0.46$  and  $0.24 \text{ \AA}^{-1}$  in case of the  $3_{10}$ -helix indicating strong curving and torsion of the backbone,  $0.40$  and  $0.15 \text{ \AA}^{-1}$  in case of the  $\alpha$  helix (intermediate curvature and torsion),  $0.36$  and  $0.08 \text{ \AA}^{-1}$  in case of the  $\pi$ -helix (weak curvature and torsion). The curvature maxima coincide with the position of the  $\text{C}_\alpha$  atoms (dots in Figure 3a,  $\kappa(s) = 0.81, 0.55$ , and  $0.45 \text{ \AA}^{-1}$ , respectively; Table 2) because they are the points of strong bending. For an  $\alpha$  helix, these points lie on the vertices of the approximate 'square' formed when the helix is seen end-on. The plane of the amide bond enforces linearity to the region in between the  $\text{C}_\alpha$  points resulting in curvature minima (Figure 3a,  $\kappa(s) = 0.28, 0.30$ . and  $0.30 \text{ \AA}^{-1}$ , Table 2).

Table 2: Curvature  $\kappa$  and torsion  $\tau$  ranges (in  $\text{\AA}^{-1}$ ) for ideal  $\alpha$ -,  $3_{10}$ -,  $\pi$ -helices, and  $\beta$ -strand structures.

Secondary units	Minimum		Maximum		Average	
	$\kappa$	$\tau$	$\kappa$	$\tau$	$\kappa$	$\tau$
$3_{10}$ -Helix	0.28	0.12	0.81	0.35	0.46	0.24
$\alpha$ -Helix	0.30	0.09	0.56	0.19	0.40	0.15
$\pi$ -Helix	0.30	0.06	0.45	0.10	0.36	0.08
$\beta$ -Strand	0.01	$< -2.90$ <sup>1</sup>	1.02	0.01	$0.38$ <sup>2</sup>	$-0.74$ <sup>2</sup>

<sup>1</sup> The value of  $\tau(\text{min})$  ranges from -13.9 to -2.9  $\text{\AA}^{-1}$ .

<sup>2</sup> Average values are given for completion. This value cannot be directly compared with the value of helices owing to the unique shape of  $\beta$  peaks. See text.

**Figure 4.** The torsion  $\tau$  is given at 20 points between two consecutive  $C_\alpha$  anchor points of the helix

backbone in dependence of the corresponding curvature values  $\kappa$  for an ideal  $3_{10}$  helix (blue points), an ideal  $\alpha$ -helix (red points), and an ideal  $\pi$ -helix (green points).

A similar reduction is found for the torsion maxima of the 3 helices (0.35, 0.19, 0.10  $\text{\AA}^{-1}$ , Table 2) reflecting the decrease in the transversion steps from 2 to 1.5, and 1.15  $\text{\AA}$ , respectively (Figure 3a,  $\tau(s)$ ). The strongest torsion is found in the peptide units because these point in the direction of the helix axis giving maximum contribution to the rise per amino acid. At the  $C_\alpha$  atoms, the torsion is at its minimum (0.12, 0.09, and 0.06  $\text{\AA}^{-1}$ , Table 2, see also  $\tau(s)$  in Figure 3a).

In addition to the  $\kappa(s)$  and  $\tau(s)$  diagrams, the characteristic differences between the three helices can be observed in a  $\kappa$ - $\tau$  diagram (Figure 4). In this case,  $\kappa(s)$  and  $\tau(s)$  are calculated for 20 points along the spline for every two successive  $C_\alpha$  atoms and are presented as function  $\kappa = f(\tau)$ . For  $3_{10}$ ,  $\alpha$ , and  $\pi$  helix, three different segregations of points are obtained where the  $3_{10}$  helix has again the largest and the  $\pi$  helix the smallest  $\kappa$ - $\tau$  values. The lack of overlap between the group of points for each helix confirms that unique values of  $\kappa(s)$  are obtained for the corresponding values of  $\tau(s)$  throughout the backbone of each helix. The sharp turning of a  $3_{10}$  helix leads to stronger oscillations in the curvature and torsion (Figure 3a), and corresponds to the wider spread of points (Figure 4). The  $\pi$ -helices, having a more relaxed structure caused by more amino acids along each turn, show the least dispersion of points. The  $\alpha$  helix takes the intermediate position as already discussed in connection with Figure 3a.

For a right-handed helix, torsion values are positive whereas they are negative for a left-handed helix: average  $\tau(s) = 0.15$  and  $-0.15$   $\text{\AA}^{-1}$ , respectively (see Figures 3a and 3b). In this way, the chirality of the helix is directly reflected by the torsion values of the protein backbone determined by APSA.

Ideal  $\beta$ -strands are regular pleats of the protein backbone, rotated along the strand axis where the majority of  $\beta$ -strands is twisted in a left-handed fashion. This is reflected in the typical patterns of the  $\kappa(s)$  and  $\tau(s)$  diagrams for the ideal  $\beta$ -strand (Figures 3c).  $\beta$ -Strands can be considered as the sterically stable conformation of a helix that has two amino acids per turn. The  $C_\alpha$  atoms lead to strong curving of the backbone line (high  $\kappa(s)$  values) but do not contribute much to the overall rise of the strand ( $\tau(s) \approx 0$ ) whereas the region in-between the  $C_\alpha$  atoms is relatively straight ( $\kappa(s) \approx 0$ ), but responsible for stretching of the strand. The turning of the spline is left-handed resulting in the strong negative torsion minima. Though the average  $\kappa(s)$  value of 0.38  $\text{\AA}^{-1}$  (Table 2) of the ideal  $\beta$ -strand is lower than that of the  $\alpha$  helix (0.40  $\text{\AA}^{-1}$ ), it should be noted that the shape and height of the  $\beta$  peaks are different. Its height, given by the difference between the maximum and minimum of each peak, is  $1.02 - 0.01 = 1.01$   $\text{\AA}^{-1}$  whereas for the  $\alpha$  helix it is  $0.55 - 0.30 = 0.25$   $\text{\AA}^{-1}$ .

Figures 3d and 3e show an  $\alpha$  helix and a  $\beta$  strand taken from a segment of natural proteins. The former structure belongs to region N51 to K63 in aspartate aminotransferase (7AAT) and reveals variations in the curvature and torsion maxima that indicate deformations of the helix. The  $\beta$ -strand from region T17 to

K23 in superoxide dismutase (2SOD) shows even more fluctuations in curvature and torsion than the ideal structure in Figure 3c. In both cases, the ends of the structures are not as perfect as their ideal counterparts. This is because they continue into neighboring turns which are non-planar. These examples emphasize that the curvature and torsion patterns are sensitive to any deformation of a real secondary structural unit. In addition, they make it possible to exactly describe entries and exits to these units, which opens up new prospects for an automated secondary structure recognition by APSA.

The three standard helices ( $3_{10}$ ,  $\alpha$ -,  $\pi$ -helix) and the  $\beta$ -strands can be distinguished by their average and extreme curvature and torsion values, as summarized in Table 2. The APSA method has been programmed to do this by utilizing the characteristic values for each structure (Table 2), whether it is in an ideally constructed polyalanine or a real protein, as will be discussed in the following sub-section. Since variation in these values is observed for  $\beta$  strands, a value of  $< -2.9 \text{ \AA}^{-1}$  is used to define the  $\tau(s)$  minimum. The various residues in the protein backbone can be appropriately determined as part of a helix or  $\beta$ -strand by defining lower and an upper limits of  $\kappa(s)$  and  $\tau(s)$  values in form of a  $\kappa - \tau$  *window* for each specific secondary structure.

### 3.1 Distribution of amino acids in ideal conformational environments

Literature is replete with comparisons of the results of various secondary structure assignment methods. It has been shown [1] that automated methods such as DSSP [4], DEFINE [12], and P-curve [13] agree in only 63 % of residues among helices,  $\beta$ -strands and non-regular structures. Additionally, it has been shown that  $\beta$ -strands showed greater disparity owing to differing definitions. [1] A recent automated assignment based on structure comparison involving STRIDE, [11] DSSP, [4] and the PDB [6] using fuzzy logic [27] revealed that the middle regions of helices show maximum agreement whereas the ends are the disputed regions. In the wake of such conflicts, it is useful to evaluate the extent of helical and  $\beta$ -strand regions that are strictly ideal in conformation. Also, rigid helices in proteins are significant in protein folding, protein-ligand and protein-protein interactions where they function as scaffolds onto which the more variable regions such as caps interact. APSA can be used to determine how many amino acids in a protein contribute to ideal conformations in secondary structures. This number reflects the conformational stability of those regions, as opposed to conformational flexibility where folding and long range interactions lead to distortions.

APSA, as discussed under section 2, is non-local and continuous in its presentation of the protein backbone and therefore it recognizes conformations reflecting global trends. An amino acid having an ideal conformation will be recognized as *ideal* only if it occurs in an ideal *environment* with a distinctive pattern in  $\kappa$  and  $\tau$  that reflect an ideal collaborative conformation. One localized  $\alpha$ -helical amino acid (having the ideal  $\phi$  and  $\psi$  value) in a region that is significantly distorted cannot be counted as an ideal  $\alpha$ -helical residue. It takes an accumulation of 3 to 4 such ideal amino acids to create a secondary structure that has the ideal  $\alpha$ -helical pitch and diameter. It is this type of pattern that APSA reads from the  $\kappa(s)$  and  $\tau(s)$  diagrams.

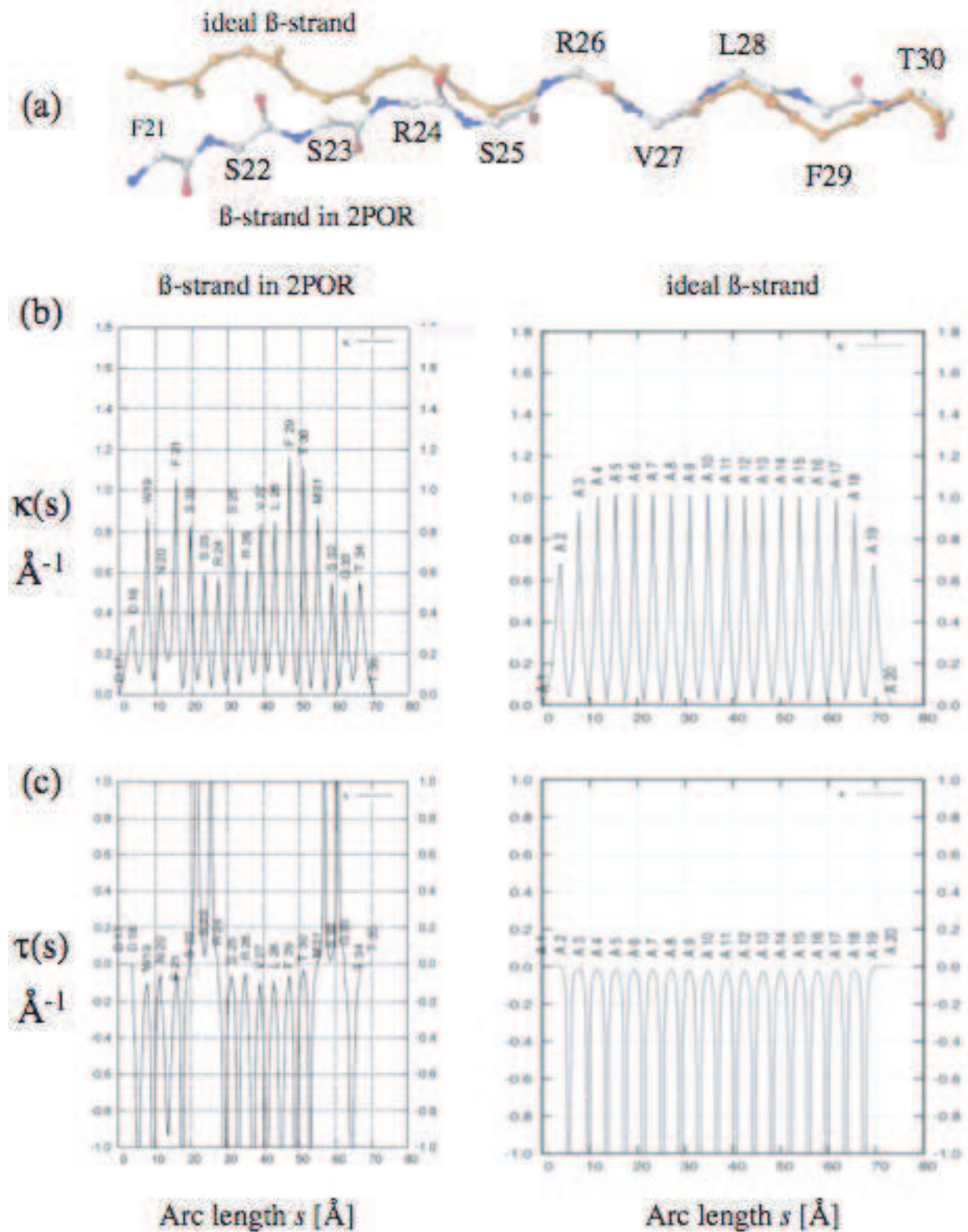
The influence of neighboring amino acids on the  $\kappa$  and  $\tau$  values of the amino acid in question, however, depends on the overall shape of the secondary structure being formed by the simplified backbone. Though it is a universal rule that this type of influence decreases with distance, drastic changes in conformation up to two  $C_\alpha$  positions away can affect the  $\kappa$  and  $\tau$  values of the amino acid in question.

Table 1 lists for 20 proteins the number of amino acids occurring in ideal environments. Results are compared with DSSP [4] as it is a widely used hydrogen bond-based method capable of recognizing  $\alpha$ ,  $3_{10}$  and  $\pi$  helices, bends, turns,  $\beta$ -strands and isolated  $\beta$ -bridges among amino acids that participate in hydrogen bonding. In the current comparison only  $\alpha$ -helices and  $\beta$ -strands longer than 2 amino acids were considered by APSA.

Among the 20 proteins, 155 helices are recognized comparable to the 159 identified by DSSP (Table 1). However, the number of residues possessing an ideal  $\alpha$ -helical conformation is lower than the DSSP number of helical residues. Out of DSSP's 1744 helical amino acids, only 65 % occurred in ideal helical environments. In some proteins such as 2FOX, 2POR, 7AAT, etc., a few helices not being recognized are not  $\alpha$ -helical in shape whereas in other proteins such as 1M8Z short helices with one or two ideal residues escape recording as the rest of the helix is distorted beyond recognition. In protein 1HC0, there is great disparity between the difference in the number of structures (5 vs 7 helices) and the ideal amino acids (26 vs 53) indicating that the protein contains helical structures of intermediate conformation between complete distortion and the ideal  $\alpha$ -helix. Though APSA recognizes in some cases (1PR, 1U4G, etc.) more helices than DSSP, this does not proportionally increase the number of ideal residues. For example for 2CTS, just 140 (54 %) out of DSSP's 257 helices are ideal. A detailed account of the various distortions found in helices with quantification of these distorted structures will be the topic of following works. [28]

The  $\beta$ -strands recognized by APSA significantly outnumber those recognized by DSSP. The disparity is because, being a geometry-based method, APSA can analyze the conformation of all amino acids in the protein and does not require the presence of the  $\beta$ -ladder. Consequently, APSA identifies more  $\beta$ -strands, but at the same time all identified  $\beta$ -strands are considerably shorter thus reflecting APSA's sensitivity with regard to any distortion. In total, the percentage of residues in an ideal  $\beta$ -environment is just 48.5. The inference that can be obtained directly from this analysis is that conformationally, the strands participating in a  $\beta$ -sheet are not as rigid as helices. The same concept has been discussed in early literature, indirectly, in terms of the inconsistency encountered when calculating and modeling hydrogen bonds into  $\beta$ -ladders [20].

The distortion of  $\beta$ -strands from ideal structure can be made visible by the superposition of one distorted example on an ideal structure as shown in Figure 5a. 2POR is a porin with the  $\beta$ -barrel architecture having 16  $\beta$ -strands with roughly 46 % of the residues being ideal. The backbone of a DSSP assigned  $\beta$ -strand from W19 to G33 is an example of a deviation from the ideal structure as a result of an overall curving of the strand and a simultaneous rotation of the backbone (as seen from the staggering of the red carbonyl



**Figure 5.** (a) A Ball&Stick representation of the backbone region W19 to G33 in 2POR (a porin; C: white; N: blue; O: red color), which deviates from a strictly ideal  $\beta$ -strand (brown color). The position of the carbonyl oxygen (red atoms) indicates torsion of the backbone besides significant backbone curvature. (b) Curvature and (c) torsion diagrams,  $\kappa(s)$  and  $\tau(s)$ , quantify deviations from the ideal  $\beta$ -strand.



oxygen atoms). The  $\kappa(s)$  and  $\tau(s)$  diagrams (Figures 5b and 5c) reveal these differences clearly (e.g., changes from left to right, back to left, then to right, and finally a left-handed torsion of the strand accompanied by varying curving) and provide a basis for discussing distortions without the need of a 3D-comparison (as done in Figure 5a). [28a]

### 3.2 Analysis of non-regular structures

From the above discussions, it is clear that the geometry-based APSA method can efficiently analyze regular repeating secondary structures. But turns are more variable and, despite several approaches used to describe them, [15] remain so far elusive to any form of classification. The term loop refers to the regions of the proteins not recognized as turns by the respective classification system used for structure description, and these regions comprise about 50 % of the protein. [15] APSA's spline fitting procedure connects all the  $C_\alpha$  points in the protein and is solely based on conformation excluding the need for any other information but the  $C_\alpha$  positions. Turns have been considered in literature [15] as a combination of helical and extended geometries. Given that protein structures are described in both ideal and real forms by APSA (Table 1), the description of turns should thus reflect the exact 3D-shape of a turn and be included in the  $\kappa(s)$  and  $\tau(s)$  diagrams of a complete protein, which will be tested in the following.

Figure 6a shows a type I turn in the backbone of ubiquitin (1UBQ, amino acids 18 to 21; colored orange in the inset). The  $\kappa(s)$  and  $\tau(s)$  diagrams of this region have the peaks of the amino acids of the turn highlighted in bold. The pattern of the turn is not a regular repeating secondary structure, however, the helical  $\tau$ -peak at proline 19 and the  $\beta$ -like  $\tau$ -peaks at E18, S20 and D 21 are recognizable. It is evident from the backbone representation that the proline is mainly responsible for the turning of the backbone and that the backbone going 'downwards' in the inset picture of Figure 6 raises a little at serine 20 before it starts going down again corresponding to the sign changes in torsion. An inspection of the other regions of the protein displayed in  $\kappa(s)$  and  $\tau(s)$  diagrams shows that the turn occurs between a regular  $\beta$ -strand to the left and a regular  $\alpha$ -helix to the right. Similarly, in Figure 6b, the type II turn from amino acid V109 to G111 (peaks in bold in the  $\kappa$  and  $\tau$  diagrams) occurs mainly at the aspartate residue at D110 where the torsion peak is helical. In this case however, in contrast to the turn example in Figure 6a, the helix is left handed as shown by the negative torsion peak at G111 and by the direction of the turn in the backbone picture. Two turn regions (both colored orange) can be recognized in the inset of Figure 6b, and the part of the  $\tau(s)$  diagram preceding the V109-G111 turn shows neither helix nor strand pattern. From the  $\kappa(s)$  and  $\tau(s)$  diagrams, it can be seen that the type II turn is followed by a  $\beta$ -strand distorted in the beginning.

Due the fact that the  $\kappa(s)$  and  $\tau(s)$  diagrams of the type shown in Figure 6 are detailed containing all the conformational information needed, similarity between proteins or parts of proteins in 3D can easily be assessed. To address this issue, 6 segments from the proteins 1JZB (variant 2 scorpion toxin), 2PAB chains A

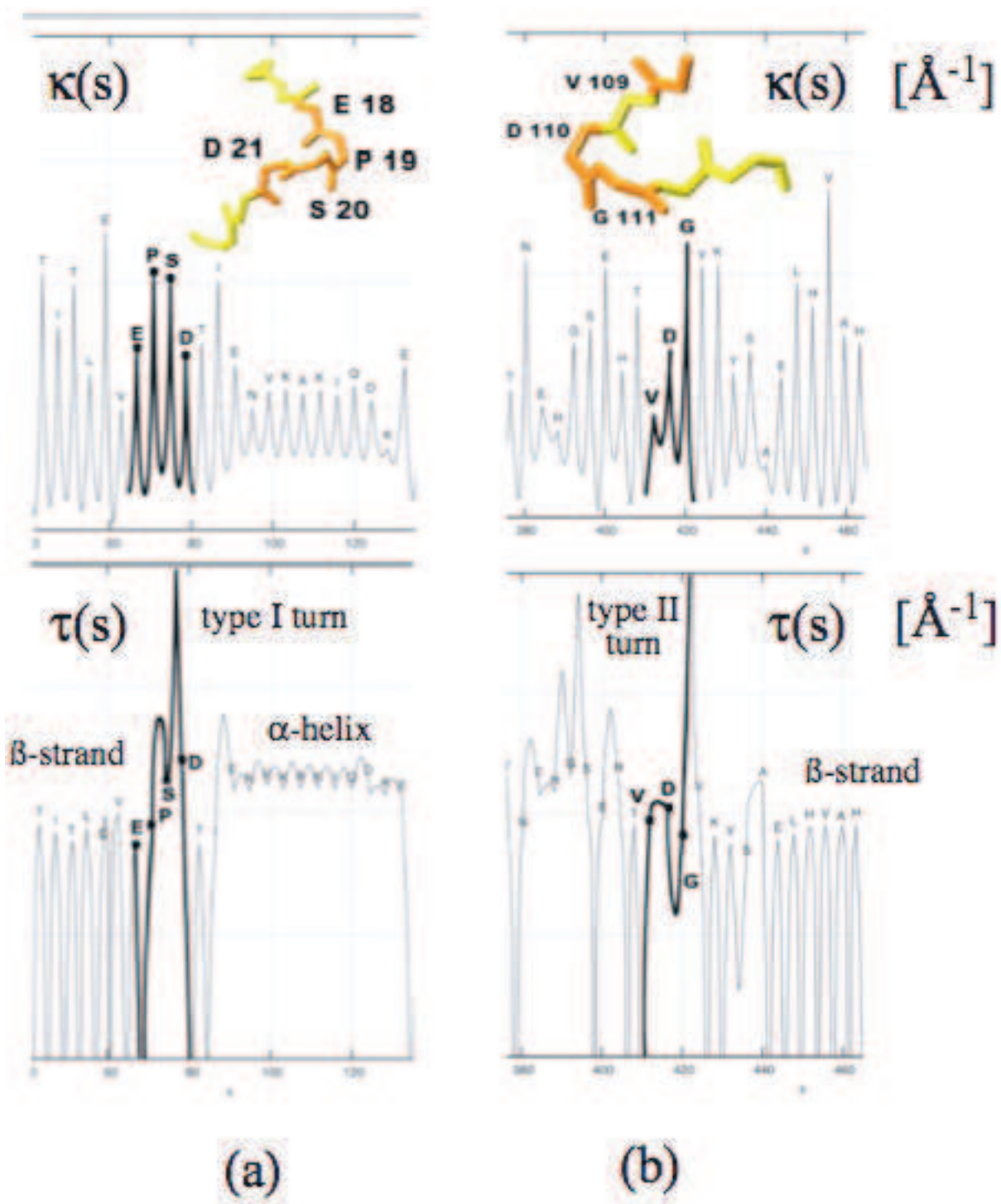


**Figure 6.** Calculated  $\kappa(s)$  and  $\tau(s)$  diagrams of (a) a type I turn as occurring in ubiquitin (1UBQ) region E18-D21, and (b) a type II turn from carbonic anhydrase form B (2CAB) region V109-V112. Insets: the backbone is colored orange in the turn regions.

& B (prealbumin), 2TPI (trypsinogen), 5PTI (bovin pancreatic trypsin inhibitor), and 7RXN (rubredoxin),

known to contain the same turn, were analyzed. The  $\kappa(s)$  and  $\tau(s)$  diagrams of these segments cut out of the respective proteins are shown in Figure 7 with a representative backbone rendering from 5PTI (inset of Figure 7). It can be seen that the  $\kappa(s)$  and  $\tau(s)$  diagrams of the turn regions are similar in all proteins both qualitatively and, to a large extent, even quantitatively.

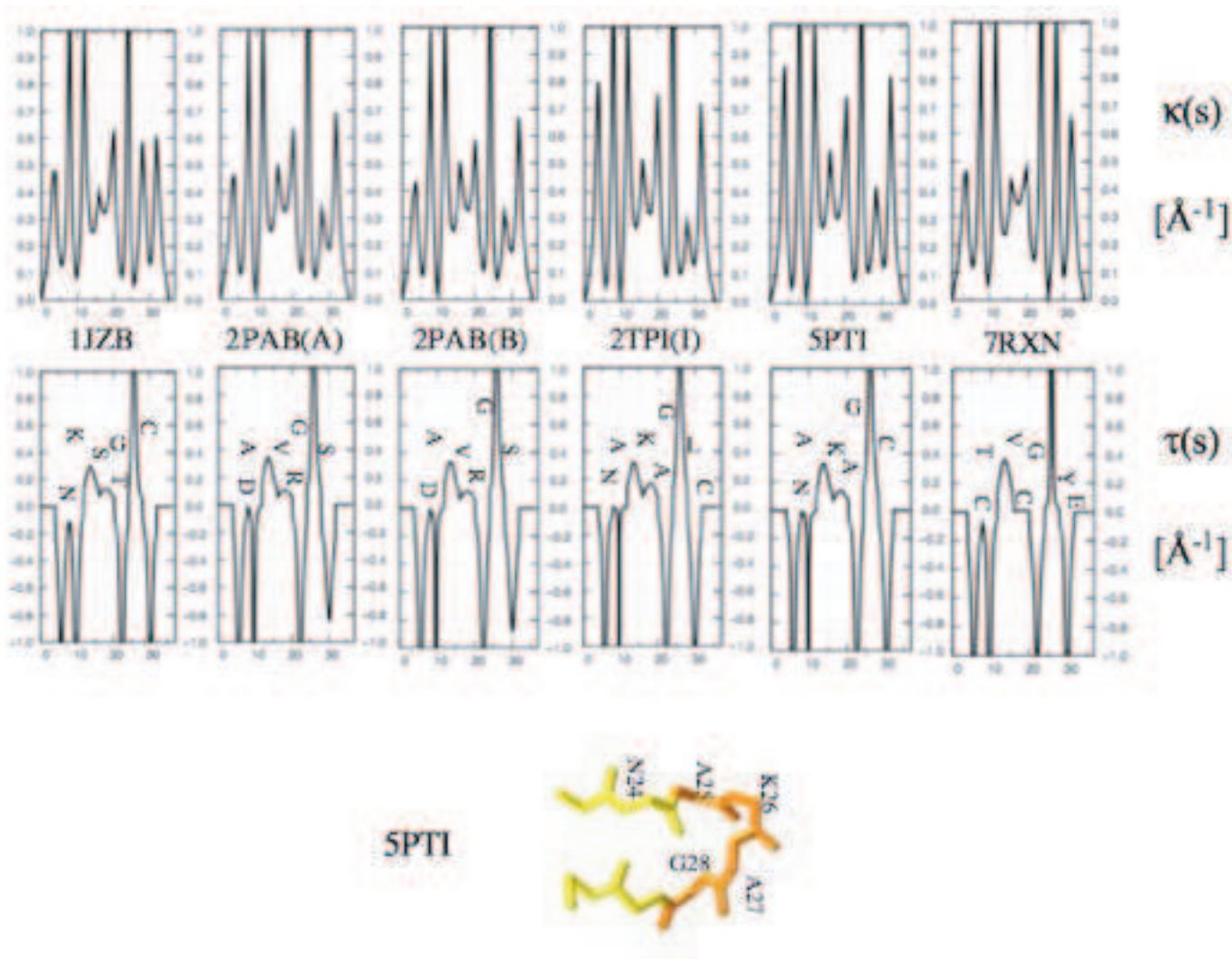


**Figure 7.** Similar conformational regions have similar  $\kappa(s)$  and  $\tau(s)$  patterns. The  $\kappa(s)$ - (above) and  $\tau(s)$ -patterns (below) of a turn region (7 residues long) that occurs in six different proteins (PDB notation [6]: 1JZB, 2PAB(A), 2PAB(B), 2TPI(I), 5PTI(I), 7RXN) is shown. The inset gives the turn region for the backbone rendering of protein 5pti.

Of the 7 residues shown in each turn (Figure 7), the first is always  $\beta$ -like (compare with Figure 3c) and extends up to the  $C_\alpha$  point of the second ( $\kappa(s)$  diagram), after which it turns helical as seen from the high minima (and short peak height) of  $\kappa(s)$  and the helix-like shape of the  $\tau(s)$  peak. This shape continues through the following residue up to the  $C_\alpha$  of the fourth. The fifth and the sixth residues are again extended,

but pointing up and down as shown by the backbone rendering and by the  $\tau(s)$  sign changes. The  $C_\alpha$  atom of the fifth residue (a glycine in all cases shown) is at the point of a sharp change in backbone orientation as shown by the strong  $\kappa(s) > 1.4$  and by the  $\tau(s)$  changing sign from strongly negative to high positive values. The turn is on the whole right-handed as revealed by the positive torsion values in the helical region (residues 2 and 3; Figure 7).

#### 4. Comparison of APSA with Related Protein Structure Description Methods

The original idea of developing APSA was based on the work with the Unified Reaction Valley Approach (URVA) of E. Kraka and D. Cremer. [29,30] There, the reaction path of a chemical reaction is presented by a curve in multi-dimensional space, which is characterized by arc length, curvature, and torsion where the latter quantities are related to energy transfer and energy dissipation during the chemical reaction. The work with URVA led to the question whether protein folding can be also described by a conformational path, in which the protein backbone changes its shape in a typical way. From there, it was just a small step to represent the backbone itself as a smooth line in 3D space, which can be characterized by arc length, curvature, and torsion.

Study of the literature revealed that related ideas have been pursued by other authors although mathematical procedures and objectives of previous work differ significantly from those of APSA. In this section, we will shortly compare previous studies based on similar ideas of describing protein structure with the work presented here.

In 1978, Rackovsky and Scheraga [31] suggested a discrete analogue to APSA to evaluate  $\kappa$  and  $\tau$  at the  $C_\alpha$  positions. The protein backbone was represented by a set of "equidistant" points in space ( $C_\alpha$  atoms) connected by virtual bonds. The four points,  $i-1, \dots, i+2$ , form an elementary unit at point  $i$  which defines  $\kappa_i$  and  $\tau_i$ . The graphical representations of  $\kappa$  vs  $\tau$  were used for identification of structural elements and diagrams giving  $\kappa$  or  $\tau$  in dependence of the residue number were employed for protein comparison. This method conforms with the local properties of curvature and torsion. The bond angles and dihedral angles defined by the virtual bonds are related to the traditional angles  $\phi$  and  $\psi$ . The virtual bonds, of course, differ significantly from the protein backbone so that  $\kappa(s)$  or  $\tau(s)$  patterns identifying structural units of a protein can no longer be obtained. Hence, the method of Rackovsky and Scheraga [31] is a forerunner of APSA based on a representation of the protein backbone by a set of discrete points, which leads to shortcomings when analyzing protein structure.

Louie and Somorjai [32,33] considered the native conformation of a protein as the collection of minimal surfaces, helicoids and catenoids, linked by turns and irregular coils, which contain mainly polar groups and are exposed to solvent. The backbone is defined as a geodesic curve on the minimum energy surface. Only helices and  $\beta$ -strands can be analyzed in this way, whereas an analysis of "non-regular" residues (belonging

to turns, loops, etc.) cannot be performed. In this approach, curvature  $\kappa$  and torsion  $\tau$  are uniformly approximated by step-wise functions corresponding to discrete values at  $C_\alpha$  atoms. The fitting produces a sequential overlap of all portions of the protein. Recognition of helices is based on the comparison with an average cylinder of given radius and pitch. The bends are recognized as changes in axial angles of the fitting helices, whereas turns are recognized when three or more consecutive changes of axial angles are each greater than  $40^\circ$ . The method cannot generally be applied and is best suited for helix recognition.

Soumpasis and Strahm [34] also considered describing the protein backbone by curvature and torsion obtained from polygonal non-differential paths defined by  $C_\alpha$  positions. At each vertex, curvature  $\kappa$  is defined from the circumscribed circle of a triangle spanned by three sequential  $C_\alpha$  atoms. Torsion  $\tau$  is defined in a similar way using a tetrahedron spanned by four  $C_\alpha$  atoms. The formulas for calculating  $\kappa$  and  $\tau$  are expressed in terms of Caley-Menger determinants. In this approach, the definition of  $\tau$  suffered from an ambiguity and, therefore it had to be augmented by an extra condition, which leads to a complex torsion with real and imaginary part. Using this approach the authors obtained specific profiles characterizing secondary and supersecondary structure. [34] One of the drawbacks of the Soumpasis-Strahm approach is that it does not produce a clear and easy-to-analyze picture of the backbone structure.

Hausrath and Goriely suggested a continuous representation of proteins from curvature profiles, [35] which were determined in a way similar to that of Louie and Somorjai. [32,33] Small segments of the protein were described by a piece of a helix, which was then used for the calculation of curvature and torsion. The latter obtained a stepwise character without specific patterns. Curvature and torsion were used for the calculation of amino acid atom coordinates in the local coordinate system. The averaged values of these coordinates were used to reconstruct the protein conformation for similarity comparisons.

Sklenar, Etchebest, and Laverrey [36] suggested a method for smoothing the protein backbone. Each residue is assigned a local helical axis system defined by a least-square-fit. The latter takes into account the differences in the axis systems of the nearest neighbors. Local variations of atomic coordinates are "smoothed" out and a more global picture can be obtained. Again, only a discrete set of points can be produced to represent the protein backbone. Differing orientations of helices are described by the method. The regions with regular secondary structures (helices and  $\beta$ -sheets) are seen as straight segments of a line, which are linked by curved segments corresponding to the non-regular conformations. This however leads to the loss of a visible difference between helices and  $\beta$ -sheets. Apart from this, structural details along the protein backbone are lost during the smoothing process. The method contains several parameters, which cannot be directly related to  $\phi$  and  $\psi$  values or to protein conformation in general.

Zhi and co-workers [37] suggested a smoothing technique for the protein backbone by averaging  $C_\alpha$  positions in a seven-residue window. Chain fragments that remain straight after smoothing are denoted as generalized secondary structure elements. The main characteristic is the turning angle along the smoothed

backbone. Analysis and comparison of protein structures can be carried out by aligning the arrays of the angles. Though this approach gives a more global view, it is unable to differentiate between secondary structural units. Can and Wang [38] estimated curvature and torsion of the protein backbone by representing it as a smooth line, which was defined by the set of  $C_\alpha$  atoms assumed to be equidistant. A 5th order spline was applied for the smoothing procedure but, contrary to the 3rd order spline used in APSA, this spline does not pass through the chosen anchor points. Helices were described with high precision, but turns were not. After subsequent normalization, the curvature and torsion were used as signature parameters for structure comparison in different proteins. No secondary structure recognition was attempted. Finally, it is noteworthy that work on DNA helices has also been carried out utilizing a description with curvature and torsion. [39,40]

## 5. Conclusions and Outlook

The description of the protein structure by its backbone is a well-accepted concept. The present work is based on this approach and presents the backbone as a smooth line in 3D space rather than a collection of discrete backbone points. The natural choice for the anchor points leading to a smooth backbone line are the  $C_\alpha$  atoms because the latter represent the flexible part of the backbone (N and C(=O) atoms are more constrained in their flexibility by the peptide bond), which directly reflects on the conformational and steric influence of the side chains. By using a continuous rather than discrete representation of the backbone we can project the 3D structure of the protein into the  $\kappa(s)$  and  $\tau(s)$  diagrams, which reveal characteristic and easy to distinguish patterns for all secondary structural units of a protein. Protein structure analysis is transferred thereby from a qualitative or semiquantitative to a quantitative level: a) Different types of helices ( $3_{10}$ -,  $\alpha$ -, or  $\pi$ -helix),  $\beta$ -strands can be easily distinguished by  $\kappa(s)$  and  $\tau(s)$  diagrams. b) The regularity of the structures can be measured and their distortions quantified. c) An analysis of amino acids occurring in ideal environments reveals that only about 63 % of DSSP's  $\alpha$ -helical amino acids and 48.5 % in the case of  $\beta$ -strands are indisputably ideal. We suggest that the disparity between various secondary structure assignment methods in the literature is partly due to this fact. d) The entire backbone can be presented as a combination of coiled and extended regions as shown for some turns.

APSA is based on the idea of subsequent steps of coarse graining the protein backbone so that more and more nonlocal features are included into the description. In subsequent work, [28,41] we have applied APSA to a whole range of tasks and problems occurring in connection with protein structure analysis. In Ref. 28a, APSA is used to analyze 533  $\alpha$ -helices and 644  $\beta$ -strands taken from 77 proteins to show how natural secondary structures differ from ideal ones. Kinks, distortions, and breaks are quantified and the boundaries (entry and exit) of secondary structures are classified. It is also shown how similar tertiary structures can be easily recognized and similarity comparisons performed by analyzing the constituting helices, strands, turns, their entries and exits. In Ref. 28, additional improvements are incorporated into the APSA protocol by

extending the test set to 155 supersecondary structures. It is shown that the function  $\tau(s)$  is sufficient to analyze the contributions of all amino acids to the conformation of the protein backbone. The characteristic peak and trough patterns of the  $\tau(s)$  diagrams can be translated into a 16-letter code, which provides a rapid identification of helices, strands, and turns, specifies entry and exit points of secondary structural units, and determines their regularity in terms of distortions, kinks or breaks. Via computer encoding, 3D protein structure is projected into a 1D string of conformational letters, which lead to words (secondary structure), combination of words to phrases (supersecondary structure), and finally to whole sentences (representation of protein chains) without losing conformational details. The 3D-1D-projection procedure represents an extension of the APSA method.

A documentation of the list of structures described by APSA leads to a library of protein subunits or building blocks that can be used in protein structure prediction and modeling. The analysis of the  $\kappa(s)$  and  $\tau(s)$  diagrams provides a meaningful and systematic way of breaking down loop regions to substructures that contribute to the library of  $\kappa$ - $\tau$  patterns. Such libraries can be used to search and classify turns, supersecondary structures, and folds in a systematic way. [41]

The definition of folds and domains is often linked to functionality, rather than to the conformation presented by the protein. Though this is aimed for far reaching goals, it leads to classification systems that are currently semi-automated, producing conflicting results with the need of reviewing them in light of new folds, as is the case with SCOP [7] and CATH [8]. APSA provides a unique way of solving this problem. At the tertiary level,  $\kappa(s)$  and  $\tau(s)$  rules can be used to recognize distinct folds, define them, and set up databanks of coordinates for each. Another important application of APSA is similarity comparison. APSA can handle rapid and accurate similarity measures at any user-defined level of coarseness: whether an exact  $C_\alpha$  to  $C_\alpha$  match or determining localized equivalent regions between the two domains. Just as any line in 3D space can be accurately and completely described by  $\kappa(s)$  and  $\tau(s)$ , the availability of latter information could lead to the reconstruction of the spline and ultimately, the backbone. In this way different segments of proteins can be put together into one continuous backbone for further computational and folding studies. For example, such studies can be performed on special proteins that undergo domain-swapping such as in the Alzheimers afflicted brain tissue. Other computational applications could include tracking, accurately and quantitatively, the conformational changes in a protein as a result of ligand binding and protein-protein interaction.

**Supporting Information available:** All curvature and torsion diagrams,  $\kappa(s)$  and  $\tau(s)$ , and the backbone line are given for each of the 20 proteins investigated in the Supporting Information.

## Acknowledgment

EK and DC thank the National Science Foundation and the University of the Pacific for support of this work.

## References

- [1] (a) Pauling, J. L.; Corey, R.B; Branson, H.R. *Proc Natl Acad Sci, USA* **1951**, *37*, 205-211. (b) Nelson, D. L.; Cox, M. M.; *Lehninger Principles of Biochemistry, 5th Edition*, Freeman, New York, 2008. (c) Mathews, C.K.; van Holde, K.E.; Ahern, K.G. *Biochemistry*, Addison, Wesley Longman, New York, 1999. (d) Anderson, C. A. F.; Rost, B. in *Structural Bioinformatics*, Bourne, P. E.; Weissig, H., Edt.s, Wiley-Liss, Hoboken, New Jersey, 2003.
- [2] Venkatachalam, C.M. *Biopolymers* **1968**, *6*, 1425-36.
- [3] Kendrew, J.C.; Bodo, G.; Dintzis, H. M.; Parrish, R.G.; Wyckoff, H.; Phillipsa, D.C. *Nature*, **1958**, *181*, 662-666.
- [4] Kabsch, W.; Sander, C. *Biopolymers*, **1983**, *22*, 12, 2577-637.
- [5] Rao S.T.; Rossman M.G. *J. Mol. Bio.* **1973**, *76*, 211-256.
- [6] Westbrook, Z.; Feng, G.; Gilliland, T. N.; Bhat, H.; Weissig, I.N.; Shindyalov, P.E. *Nucleic Acids Research* **2000**, *28*, 235-242.
- [7] Murzin, A.G.; Brenner, S.E.; Hubbard, T.; Chothia, C. *J. Mol. Biol.* **1995**, *247*, 536-540.
- [8] Orengo, C.A.; Michie, A.D.; Jones, S.; Jones, D.T.; Swindells, M.B.; Thornton, J.M. *Structure* **1997**, *5*, 1093-1108.
- [9] Dietmann, S.; Holm, L. *Nat. Struct. Biol.* **2001**, *8*, 953-957.
- [10] Day,R.; Beck, D.A.; Armen, R.S.; Daggett, V. *Protein Science* **2003**, *12*, 2150-2160.
- [11] Frishman, D.; Argos, P. *Proteins*, **1995**, *23*, 566-579.
- [12] Richards, F.M.; Kundrot, C.E. *Proteins*, **1988**, *3*, 71-84.
- [13] Martin, J.; Letellier, G.; Marin, A.; Taly, J.F.; Brevern, A.; Gibrat, J.F. *BMC Structural Biology*, **2005**, *5*, 17.
- [14] Efimov, A.V.*Prog. Biophys. Molec. Biol.* **1993**, *60*, 201-239.
- [15] Richardson J., *Adv in Prot Chem.* **198**, *34*, 167-339.
- [16] Raveh, B.; Rahat, O.; Basri, R.; Schreiber, G. *Bioinformatics*, **2006**, *23*, e163-e169.



- [17] Salamov, A.A.; Solovyev, V.V. *J. Mol. Biol.* **1995**, *247*, 11-15.
- [18] Kister, A.E.; Phillips, J.C. *Archiv.org, e-Print Archive, Condensed Matter* **2008**, 1-17.
- [19] Bower, M.J.; Cohen, F.E.; Dunbrack, R.L. *J. Mol. Biol.* **1997**, *267*, 1268-1282.
- [20] Mattos, C.; Petsko, G.A.; Karplus, M. *J. Mol. Biol.* **1994**, *238*, 733-747.
- [21] Jones, D.T. *The Pharmacogenomics J.* **2001**, *1*, 126-134.
- [22] Benedetti, E.; Blasio, B.D.; Pavone, V. Pedone, C.; Santini, A.; Crisma, M.; Toniolo, C. *Molecular Conformations and Biological Interactions*, Indian Academy of Sciences, Bangalore, 1991, p. 497-502.
- [23] Emberly, E.G.; Mukhopadhyay, R.; Wingreen, N.S.; Tang, C. *J. Mol. Biol.* **2003**, *327*, 229-237.
- [24] Kreyszig, E. *Differential Geometry, Dover Publications*, London, 1991.
- [25] Neumaier, A.; Dallwig, S.; Huyer, W.; Schichl, H. *New techniques for the construction of residue potentials for protein folding: Algorithms for Macromolecular Modeling. Lecture Notes Comput. Sci. Eng.* 4, Leimkuhler, B.; Chipot, C.; Elber, R.; Laaksonen, A.; Mark, A.; Schlick, T.; Schütte, C.; Skeel, R., Eds., Springer, Berlin 1999, 212-224.
- [26] Tung, C.-H.; Huang, J.-W.; Yang, J.-M. *Genome Biology* **2007**, *8*, R31.
- [27] Arab S.; Didehvar, F.; Saleghi, M.; *Iranian J. Biotech.* **2007**, *5*, 93-99.
- [28] (a) Ranganathan, S.; Izotov, D.; Kraka, E.; Cremer, D. *Proteins: Structure, Functions, and Genetics*, submitted. arXiv:0811.3034v2 [q-bio.QM]. (b) Ranganathan, S.; Izotov, D.; Kraka, E.; Cremer, D., arXiv:0811.3258v2[q-bio.QM].
- [29] Konkoli, Z.; Kraka, E.; Cremer, D. *J. Phys. Chem. A* **1997**, *101*, 1742.
- [30] Kraka, E. in *Encyclopedia of Computational Chemistry*, Schleyer, P.v.R.; Allinger, N.L.; Clark, T.; Gasteiger, J.; Kollman, P.A.; Schaefer III, H.F.; Schreiner, P.R. Eds. John Wiley, Chichester, UK, 1998, Vol. 4, p.2437.
- [31] Rackovsky, S.; Scheraga, H.A. *Macromolecules*, **1978**, *11*, 1168-1174.
- [32] Louie, A.H.; Somorjai, R.L. *J. Mol. Biol.* **1983**, *168*, 13-162.
- [33] Louie, A.H.; Somorjai, R.L. *J. Theor. Biol.* **1982**, *98*, 189-209.
- [34] (a) Soumpasis, D.M.; Strahm, M.C. *J. Biomolecular Structure and Dynamics* **2000**, *17*, 965-979. (b) Soumpasis, D.M.; Strahm, M.C. *Structure, Motion, Interaction and Expressions of Biological Macromolecules*, Proceedings of the Tenth Conversation, State University of New York, Albany, NY 1998, 11-32.
- [35] Hausrath, A. C.; Goriely, A.; *J. Struct. Biol.* **2007**, *158*, 267-281.

- [36] Sklenar, H.; Etchebest, C.; Laveray, R. *Proteins: Structure, Functions, and Genetics*, **1989**, *6*, 46-60.
- [37] Zhi, D.; Krishna, S.; Cao, H.; Pevzner, P.; Godznik, A. *BMC Bioinformatics*, **2006**, *7*, 460.
- [38] Can, T.; Wang, Y.-F. *J. Bioinformatics and Comp. Biol.* **2004**, *2*, 215-239.
- [39] Goyal, S.; Perkins, N.C.; Lee, C.L. *J. Comp. Phys.* **2005**, *209*, 371-389.
- [40] Goyal, S.; Lillian, T.; Blumberg, S.; Meiners, J.-C.; Meyhofer, E.; Perkins, N.C. *Biophys. J.* **2007**, *93*, 4342-4359.
- [41] Ranganathan, S.; Izotov, D.; Kraka, E.; Cremer, D., arXiv:0811.3464v2 [q-bio.QM]

## APPENDIX I

For the purpose of determining the number of amino acid residues influenced by the natural boundary conditions, a test was performed on 1HVZ, a circular polypeptide taken from the PDB [6]. This cyclic protein with 18 amino acids (residue 18 is connected to residue 1; see Figure A1) was analyzed treating residue 1 (and 8) both as a terminal and as a central residue. For this purpose the analysis was started as residue 1 and performed through residues 2,  $\dots$ , 8,  $\dots$ , 18, 1,  $\dots$ , and stopped at residue 8 being now a terminal residue, i.e. residue 1 (8) functioned both as a terminal and central residue.

A comparison of the curvature of the repeated regions (Figures A1a) and A1b)) reveals the error due to boundary conditions. Curvature and torsion for the first two residues differ significantly whereas the error for the third residue is relatively small. This is confirmed for the backbone line of 1HVZ shown in Figure A1c. The spline lines of the two passes in regions G1 to R8 coincide with the exception of the parts G1-F2 (start of the analysis) and C7-R8 (termination of the analysis). It was inferred that the spline is reliably described from the third amino acid onwards whereas errors for the residue next to the terminal one are moderate, however substantial for the terminal residue itself. We will exclude therefore terminal and the two next-to-terminal residues of a protein from the analysis.

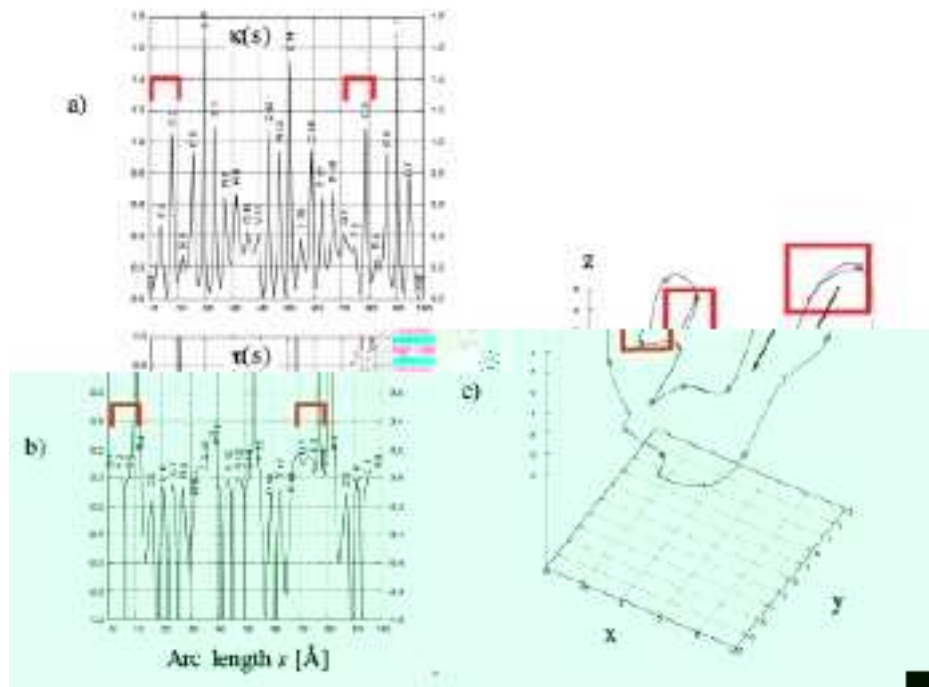


**Figure A1:** Curvature and torsion analysis for the cyclic polypeptide 1HVZ. a) Curvature diagram, b) torsion diagram, and c) backbone line for a pass from residue 1 thru residues 2,  $\dots$ , 8,  $\dots$ , 18, 1,  $\dots$ , 8 (see text). The region of deviations due to the boundary conditions are given in red.